DNA Origami Compliant Nanostructures with Tunable Mechanical Properties

Lifeng Zhou, Alexander E. Marras, Hai-Jun Su,* and Carlos E. Castro*

Department of Mechanical and Aerospace Engineering, The Ohio State University, Columbus, Ohio 43210-1286, United States

ABSTRACT DNA origami enables fabrication of precise nanostructures by programming the self-assembly of DNA. While this approach has been used to make a variety of complex 2D and 3D objects, the mechanical functionality of these structures is limited due to their rigid nature. We explore the fabrication of deformable, or compliant, objects to establish a framework for mechanically functional nanostructures. This compliant design approach is used in macroscopic engineering to make devices including sensors, actuators, and robots. We build compliant nanostructures by utilizing the entropic elasticity of single-stranded DNA (ssDNA) to locally bend bundles of double-stranded DNA into bent geometries whose curvature and mechanical properties can be tuned by controlling the length of ssDNA strands. We demonstrate an ability to achieve a wide range of geometries by adjusting a few strands in the nanostructure design. We further developed a mechanical model to predict both geometry and mechanical properties of our compliant nanostructures that agrees well with experiments. Our results provide a basis for the design of mechanically functional DNA origami devices and materials.

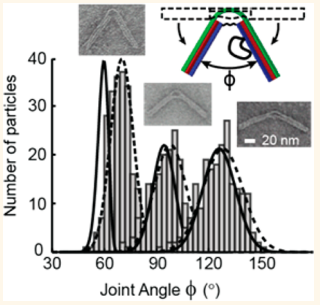

KEYWORDS: DNA origami · nanotechnology · compliant mechanisms · mechanical modeling · self-assembly

DNA origami is an emerging nanotechnology that uses DNA as material to create various nanostructures by programming its self-assembly through nucleotide sequence design.[1−6] While DNA itself is relatively flexible as a biopolymer, in DNA origami, many DNA strands are folded into a mechanically stiff structure that maintains a well-defined geometry. In particular, scaffolded DNA origami[3,7] has enabled the fabrication of nanoscale objects with unprecedented 3D geometric complexity. With this approach, a long single-stranded DNA "scaffold" strand is folded into compact geometry by long-range interactions that are programmed according to the piecewise base-pairing complementarity of many shorter "staple" strands. In recent years, scaffolded DNA origami has been used to fabricate a variety of 2D and 3D structures for functional applications,[8] such as nanopores for single-molecule sensing,[9] nanoscale containers for drug delivery,[10,11] nanotubes for structural alignment,[12] or molecular platforms for templating nanoparticles,[13,14] nanotubes,[15] or proteins.[16] These structures demonstrate the immense potential of DNA origami nanofabrication for a range of applications in fields including single-molecule biophysics, structural biology, and biomedicine.

DNA origami nanostructures contain several thousand base pairs arranged into objects with typical dimensions of ∼10−100 nm. Since spatial registry is largely retained over every base pair in the object, chemical functionalities can be placed on objects with approximately nanometer resolution. Current applications of DNA origami exploit this precise geometric design. Furthermore, computer-aided design programs, such as caDNAno,[17] have been developed to simplify the sequence design process, and the finite-element-based software, CANDO, was developed to predict the folded geometry of scaffolded DNA origami structures,[7,18] which is particularly useful when designing structures that incorporate local stresses to create curved or twisted objects.[4] These computer-aided design tools facilitate rapid prototyping of designed DNA nanostructures.[19−22] The demonstrated applications have fostered a growing interest in building DNA-based devices, machines, and robots.[10,23−26] However, applications of DNA origami to date have largely focused

* Address correspondence to castro.39@osu.edu, su.298@osu.edu.

Received for review October 16, 2013 and accepted December 18, 2013.

Published online December 18, 2013
10.1021/nn405408g

on geometric design. The fabrication of mechanically functional structures such as springs, actuators, and manipulators, which could greatly broaden the scope of DNA nanomachines, has remained largely unexplored.

In general, mechanical functionality requires two key capabilities: (1) an ability to specifically design mechanical behavior and (2) the ability to integrate dynamics (*i.e.*, motion). In engineering design, controllable mechanical behavior is achieved by using multiple material components with the desired mechanical stiffness. The stiffness of DNA origami components can vary over several orders of magnitude from highly flexible single-stranded DNA (ssDNA), which exhibits a persistence length of ~2 nm,[27] up to bundles of double-stranded DNA (dsDNA), which can be 1000-fold stiffer.[28] However, while theoretical models have provided effective and convenient methods to analyze the behavior of double helical nucleic-acid structures,[19−22] predictive models to guide the design of mechanical properties of DNA origami nanostructures are lacking, and integrating multiple DNA components to achieve tunable mechanical behavior has not been explored. Furthermore, achieving controlled dynamic behavior in designed DNA systems remains a key challenge in the field. This is usually done in macroscopic systems by integrating flexible elements with constrained motion (*i.e.*, joints), but flexibility in nanoscale systems leads to random thermal motion.[29]

One promising approach to achieve controlled mechanical and dynamic behavior with stiff components that has been successfully applied for microscopic machines[30,31] is compliant mechanism design. Compliant mechanisms[32,33] utilize components with varying stiffness and geometry to achieve controlled motion. This approach requires an ability to design components with controllable mechanical behavior and geometry. Here we establish a foundation for DNA origami compliant mechanisms by designing, fabricating, and characterizing a deformable (compliant) DNA origami nanostructure with controllable geometry and mechanical behavior.

RESULTS

Design of DNA Origami Compliant Joint. The structure was designed to behave as a compliant joint similar to a hinge with a torsional spring. Our design was constructed as an 18-helix bundle that was organized into three layers of six helices (Figure 1). The two ends, which contain all 18 helices, are stiff components that could be integrated into a larger-scale mechanism. The central portion, which forms the basis of the compliant joint, consists of the top layer of 6 dsDNA helices (green in Figure 1) and 6 ssDNA connections across the bottom layer (blue in Figure 1). The ssDNA connections function as entropic springs that apply a force causing the top layer to bend. The magnitude of the force, and correspondingly the joint angle (ϕ), depends on the

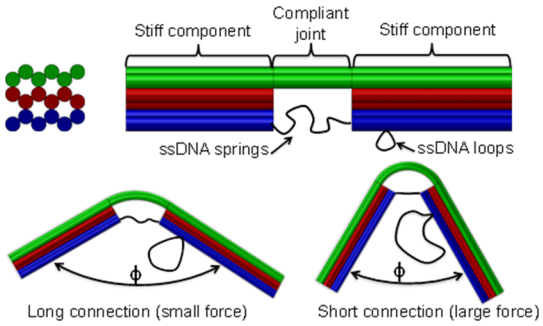

Figure 1. Three-dimensional model and function of DNA origami compliant nanostructure. The structure is an 18-helix bundle organized into 3 layers (top left). The two ends that contain all 18 helices are stiff components that could be integrated into a larger mechanism. The central portion balances tension in the ssDNA "springs" with bending of the top 6-helix layer. The joint angle, ϕ, can be adjusted by shifting length of ssDNA between the springs and the loops.

length of the ssDNA springs. In a bent configuration, the ssDNA springs connecting the top 3 helices of the blue layer span a larger distance than the ssDNA springs connecting the bottom 3 helices of the blue layer. Therefore, the ssDNA connections between the top three helices were correspondingly made longer. For subsequent definition, we refer to the length of the shorter ssDNA springs. Complete design details of all versions are given in Supporting Information Table S2.

We developed a novel approach to modulate the structural and mechanical properties using scaffold loops as a reservoir of additional ssDNA length (Figure 1, top right). The combined number of ssDNA bases in the springs and loops remained constant. Small joint angles could be obtained by shifting length from the ssDNA springs to the reservoir loops, and in contrast, large angles could be obtained by shifting ssDNA from the loops to the springs. In this way, structures with distinct geometries (joint angles) could be achieved by switching out only the staples located between the loops and the springs. We optimized our scaffold routing to minimize the possibility of secondary structure[34,35] in the ssDNA springs. For cases of small joint angles, where the ssDNA loops were long, short staples (~20 bases) were added to minimize the possibility of multiple structures interacting at the single-stranded loops.

Agarose gel electrophoresis (Figure 2a) and TEM images of the five versions (Figure 2b−f) confirm that longer ssDNA springs result in larger joint angles. In many cases, the details of the compliant joint (6-helix layer and gap between the other two layers) are visible. Aside from the smallest angle version, all of the structures adopt a smooth curvature that depends on the force applied by the ssDNA springs. In the case of the smallest angle, some structures adopt a kinked configuration (Figure 2b and Supporting Information, Figure S6a). This can be explained by the existence of nicks that occur at the staple cross-overs in the 6-helix layer of the compliant joint. Kinks occur at nicks due to reduced stiffness.[36]

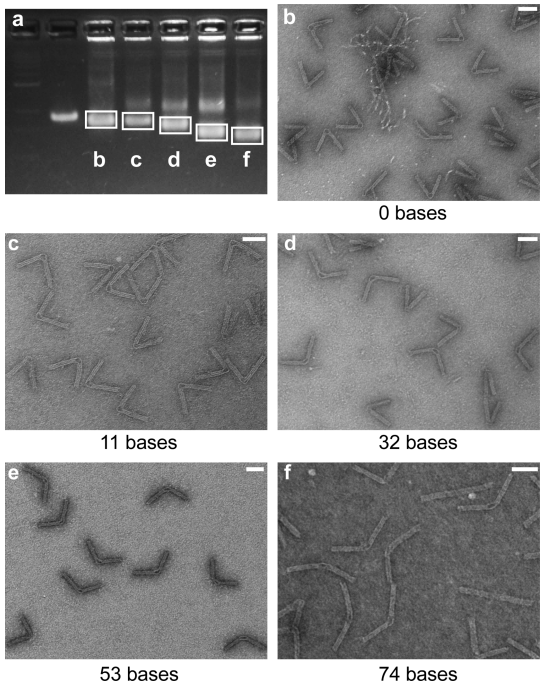

Figure 2. TEM experimental results. (a) Gel electrophoresis reveals geometric differences between design versions. The bands from left to right are as follows: DNA ladder, ssDNA scaffold, and five design versions with 0, 11, 32, 53, and 74 bases in the ssDNA springs on the following five columns. (b−f) TEM images of the five design versions. Scale bars, 50 nm.

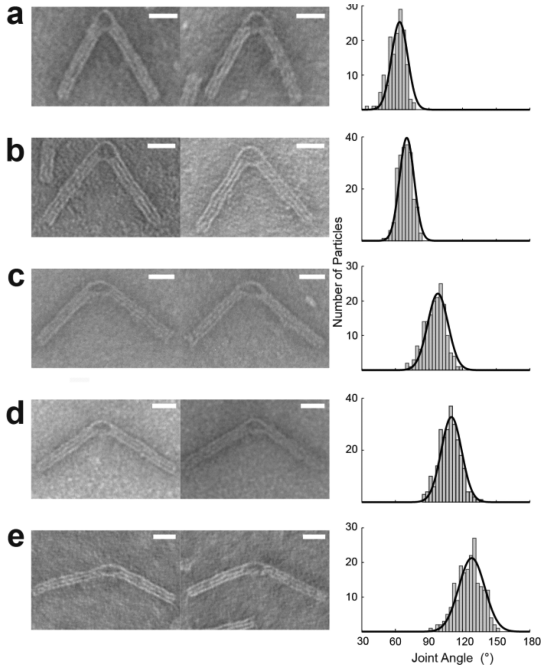

Figure 3. Conformational analysis of the TEM experiment results. (a−e) Typical particles and histogram distribution of versions with 0, 11, 32, 53, and 74 bases in the ssDNA springs. The black lines show Gaussian fits to the data. The angles corresponding to the peak values of Gaussian fits were 56.5° (n = 154), 70.2° (n = 213), 97.9° (n = 169), 110.0° (n = 252), 128.2° (n = 204). All scale bars are 20 nm.

The software ImageJ was used to manually measure the angles of each structure from TEM images. The standard deviation of the manual measurement was found to be 1.2° (Supporting Information, Figure S5). To ensure measurement of properly folded structures, only the particles with a smooth curved segment and an obvious gap between the other two layers were included in the analysis. A Gaussian distribution was used to fit the angular distributions of each version (Figure 3). The angles corresponding to the peak value of the Gaussian fits ranged from ∼55 to ∼130°, and correspondingly, the bending angles of the curved segment ranged from about ∼125 to ∼50°. The angular distributions also revealed that longer ssDNA springs resulted in larger variation in the joint angle, suggesting a lower joint stiffness (Figure 2 and Supporting Information, Figure S6). Due to thermal fluctuations, the compliant joint fluctuates about the equilibrium angle, which occurs when the extensional energy in the springs balances the bending energy in the 6-helix layer. The entropic elasticity of the ssDNA exhibits higher stiffness at larger extension, or larger angles, resulting in a slight asymmetry of the angular distribution (steeper gradient at larger angles).

Theoretical Model of Balanced Bending and Entropic Tension. Some previous efforts have examined the mechanical behavior of biopolymers with internal bends or discontinuous mechanical behavior.[37,38] While these models are useful to understand the thermal fluctuations of complex biopolymers that are qualitatively similar to our compliant nanostructures, here our goal was to develop a model capable of predicting both the equilibrium angle and the full angular distribution based purely on the mechanical properties and geometry of the constituent ssDNA and dsDNA. We envision that this model can be used as a design tool for compliant DNA origami joints. We developed a theoretical model using a flexible polymer (persistence length, L_p, is much less than the contour length, L_c) wormlike chain (WLC) model[39] for the ssDNA springs and a beam model for the 6-helix layer (Figure 4a). The Marko−Siggia analytical approximation to the WLC[22] shown in eq 1 was used to describe the ssDNA springs.

$$F_{WLC}(L_c, x) = \frac{k_B T}{L_p}\left[\frac{1}{4\left(1-\frac{x}{L_c}\right)^2} - \frac{1}{4} + \frac{x}{L_c}\right] \quad (1)$$

Here L_c is the contour length and x is the extension. The smallest angle version with the shortest ssDNA springs violates the flexible polymer assumption and in some cases exhibited kinks rather than smooth curvature in the joint. Hence, it was excluded from this analysis.

The tension in the ssDNA entropic springs creates a force that causes bending of the 6-helix layer. In the analytical model, a short rigid bar (line AB in Figure 4a) was used to account for the offset in the bending force applied by the ssDNA. We assumed that the

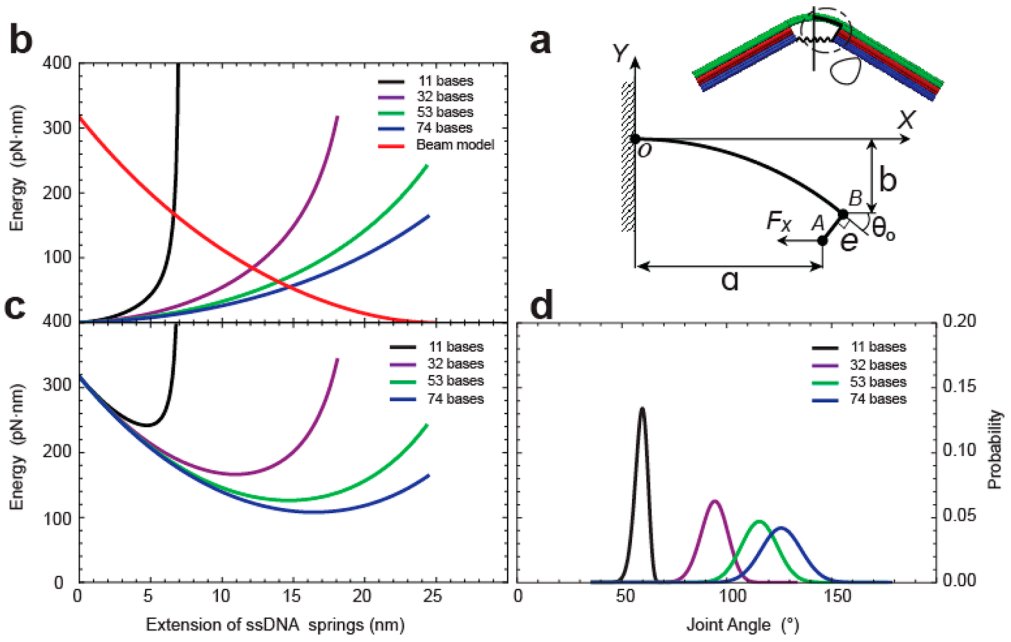

Figure 4. Theoretical model of the compliant joint. (a) Beam model of the curved segment. (b) Energy stored in the 6-helix layer (red) due to bending and in the 11 (black), 32 (purple), 53 (green), and 74 (blue) bases long ssDNA springs based on a WLC model. (c) Total energy of the compliant joint is the sum of the bending energy in the 6-helix layer and the extensional energy of the ssDNA springs. (d) Energy landscapes were used to predict Boltzmann distributions of the thermal fluctuations in angles.

deformation of the curved segment was symmetric since both the geometry of the compliant joint and the horizontal force from the ssDNA are symmetric. The rest of the structure can be viewed as rigid since it consists of the full 18-helix cross section. The 6 helices of the dsDNA layer in the compliant joint were modeled as six cylinders bonded together in parallel (Supporting Information, Figure S1). The bending stiffness of the 6-helix layer is defined as EI, where E is the elastic modulus and I is the cross-sectional moment of inertia. To find EI for the 6-helix layer, we first determined the EI of dsDNA based on a persistence length of 50 nm[22,40−42] ($L_p = EI/k_BT$) and then scaled EI according to the increase in I for the bundle (Supporting Information). The bending energy of the 6-helix layer was calculated using Euler−Bernoulli beam theory (Supporting Information, eqs S1−S9). Euler−Bernoulli beam theory was first used to calculate the deformation of the beam (Supporting Information, eqs S1−S8). The internal bending moment along the beam, $M(s)$ (Supporting Information, eq S2), was then used to calculate the energy stored in the beam[43] according to

$$E_{beam} = \int_0^L \frac{M^2(s)}{2EI} ds = W_{ex} \quad (2)$$

Here W_{ex} is the work done by the external loads applied to the beam, which in this case consists of the force from the ssDNA springs.

The extensional energy stored in the ssDNA springs was calculated by integrating eq 1 over the interval from zero to the extension of the ssDNA springs (Supporting Information, eqs S10−S14).

We defined the deformation of the compliant joint in terms of the end-to-end distance of the ssDNA springs, r ($r = 2a$ in Figure 4a). As shown in Figure 4b, the minimum energy configuration of the springs occurs at $r = 0$, and the minimum energy configuration for the 6-helix layer occurs when r is equal to the length of the 6-helix layer, L_0. The total energy of the compliant joint, $U(r)$, is obtained by summing the energy of the 6 ssDNA springs and the energy stored in the bent beam (Figure 4c). Based on the relation between ϕ and a described by eqs S6 and S7 in Supporting Information, $U(\phi)$ could be easily obtained. The equilibrium angle of the compliant joint occurs at the minimum total energy configuration. The equilibrium angles calculated from the analytical model were 59.8, 94.4, 115.6, and 126.0° for the 11, 32, 53, and 74 base long ssDNA springs, respectively. Figure 5a compares the equilibrium angles predicted by our analytical model to the equilibrium angles from the experimental distributions. Note that our model is purely predictive and does not contain any fitting parameters.

Evaluating and Predicting Joint Stiffness. Due to thermal fluctuations, the compliant joint will fluctuate about this equilibrium position. The magnitude of the thermal fluctuations is proportional to the stiffness of the joint. Angular distributions (Figure 4d) were calculated from the analytical energy landscapes of the compliant joint (Figure 4c) using Boltzmann distribution, $P(\phi) = \exp(-U(\phi)/k_BT)/Z$, where k_B is Boltzmann's constant, T is the absolute temperature, and Z is the partition function defined as $Z = \int_{-\infty}^{\infty}\exp(-U(\phi)/k_BT)d\phi$. The angular distributions are wider for longer ssDNA

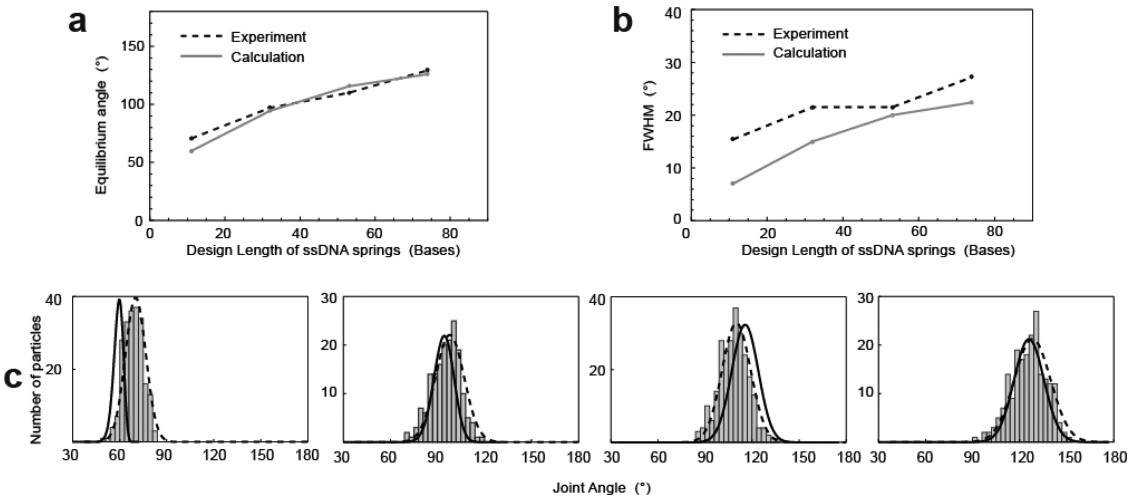

Figure 5. Theoretical model captures angular distribution. (a) Theoretical model closely captures the equilibrium angles and (b) trend of increasing width, characterized by the fwhm, of the distributions with longer ssDNA springs. (c) Full angular distribution (black), calculated using a Boltzmann distribution of our analytical energy landscape, also captures the asymmetry of the experimental distributions (gray). Gaussian fits are also shown in dashed black.

springs, which is consistent with the angular distributions shown in Figure 3. This implies that the torsional stiffness of the compliant joint decreases while the joint angle increases.

Figure 5b compares the full width at half-maximum (fwhm) value calculated from our theoretical energy distributions to the fwhm of the experimental distributions. Figure 5c compares the full distributions. Even without any fitting parameters, our theoretical model captures the trend of increasing thermal fluctuations with longer ssDNA springs and also captures the asymmetry of the angular distributions, which results from the asymmetric energy landscape (Figure 4c).

DISCUSSION

We have introduced a novel approach to design mechanically functional DNA origami nanostructures. The nanostructure functions as a compliant joint where the geometry and mechanical properties are determined by a balance of tension in flexible ssDNA components and bending in structurally well-defined dsDNA bundles. We further developed a novel approach to tune the geometry and mechanical properties of the DNA nanostructure by introducing ssDNA scaffold loops that functioned as a reservoir to add or remove length from ssDNA components. Five different structures with joint angles ranging from 56.5 to 128.2° were achieved simply switching out a small subset (15%) of the overall number of staples.

In order to quantitatively understand the behavior of the compliant joint, an analytical model (Supporting Information) was developed that combined a beam model and an entropic model (WLC) of the stiff (dsDNA bundle) and flexible (ssDNA) segments, respectively, of the compliant joint. This analytical model closely captured the equilibrium joint angles and the angular distributions resulting from thermal fluctuations of the four design versions with appropriate lengths of ssDNA. The analytical model also captured the trend of increasing magnitude of thermal fluctuations with longer ssDNA springs, indicating that the stiffness of the compliant joint is also tunable. To test the validity of our model, we explored a simple alternative, using a torsional spring to replace the beam description in the compliant joint model. The results show that the beam model better predicts the experimental results over the entire range of designs (Supporting Information, Figure S4).

In order to estimate the torsional stiffness of the compliant joint, it can be approximated as a linear torsional spring that follows the equation $T = \kappa\Delta\theta$, where $\Delta\theta$ is the change in angle from the equilibrium angle, κ is the torsional stiffness, and T is the torque required to deform the angle by $\Delta\theta$. In this case, κ can be related to thermal energy by the theorem of equipartition of energy as $\kappa\langle\Delta\theta^2\rangle = k_BT$. Based on the joint angle variance, $\langle\Delta\theta^2\rangle$, calculated from experimental distributions, we determined torsional stiffness ranging from 107 pN·nm/rad for the longest ssDNA spring up to 367 pN·nm/rad for the shortest ssDNA spring. These results indicate that we can design compliant joints with torsional stiffness similar to or stiffer than actin binding proteins such as Arp 2/3 (~80−130 pN·nm/rad)[44] or Filamin (~50 pN·nm/rad).[45] Since the persistence length of DNA origami nanostructures is also tunable over several orders of magnitude up to >micrometers, DNA origami could ultimately be used to design biomaterials with mechanical behavior similar to cross-linked actin networks.[46−48]

We demonstrated an ability to tune the geometry and stiffness of a DNA origami compliant joint with a novel approach of locally shifting single-stranded scaffold DNA within the structure. By this parameter alone, the geometry and stiffness cannot be controlled

independently. Longer ssDNA springs results in larger joint angles with lower torsional stiffness. However, our model includes additional design parameters, specifically the length and bending stiffness of the stiff component, here a layer of 6 dsDNA helices. By cooperatively adjusting the three design parameters of the compliant joint (length of the stiff dsDNA component, bending stiffness of the stiff dsDNA segment, and length of ssDNA springs), both the bending stiffness and the joint angle could be independently designed. For example, our theoretical model predicts that an 8-helix layer as the stiff segment with 28 base long ssDNA springs would give a similar equilibrium joint angle but narrower distribution to the 6-helix layer with 32 bases (Supporting Information, Figure S2a). Similarly, different joint angles with the same stiffness can be achieved by cooperatively varying the bending stiffness of the top layer (*i.e.*, number of helices) and the length of the ssDNA springs (Supporting Information, Figure S2b). Tuning the properties of the stiff segment, unlike adjusting the length of the ssDNA springs, would require designing a new structure. Nonetheless, the analytical model presented here could be used as a tool to guide the design of compliant joints with a wide range of joint angles and torsional stiffness.

A range of values have been reported in previous literature for some of the parameters used in our model including the length of a ssDNA base,[49−51] the persistence length of ssDNA,[27,52] the length of a dsDNA base pair,[22,53,54] and the persistence length of dsDNA.[22,40−42] Therefore, we checked the sensitivity of our model to these parameters (Supporting Information, Figure S3). Variation in the length of ssDNA or dsDNA had minimal effect. Variation within the reported range of values of the persistence length of ssDNA and dsDNA, which largely determine the stiffness parameters in our model, both caused similar variations of ∼10−15° in joint angle and ∼2−4° in fwhm. The offset distance of ssDNA springs from the curved segment also results in a higher sensitivity to the equilibrium angle due to its influence on the moment applied to the curved segment. While the numerical results are somewhat sensitive to the values used, the qualitative trends and conclusions drawn are not.

Here we presented the first demonstration of a compliant (deformable) DNA origami nanostructure with geometry and stiffness that can be designed according to a theoretical micromechanical model. Previous work to create controllable curvature in DNA origami nanostructures was either designed on an ad hoc basis[6] or followed a mechanical model that predicted only geometry.[4] The finite-element-based software, CANDO,[18] is a useful computational tool to predict the folded geometry and thermal fluctuations of curved or twisted structures; however, a theoretical model that directly predicts the joint angles and mechanical behavior provides a more convenient tool to quickly optimize design of compliant joints for desired structural and mechanical behavior.

Our approach establishes a foundation to design and fabricate DNA-based devices with mechanically functional components such as springs, joints, or actuators. Ultimately, compliant components like the ones presented here can form the basis of compliant mechanisms that can be applied as nanomechanical devices with controllable motion.

MATERIALS AND METHODS

Producing ssDNA Scaffold. The scaffold used in this work is a 7560 base clone of the M13MP18 bacteriophage virus.[5] The scaffold was produced in our lab following protocols detailed in Castro *et al.*[7] Full details are provided in the Supporting Information.

DNA Origami Structure Design and Fabrication. The structure and staple sequences were designed using the DNA origami computer-aided design software caDNAno[17] and fabricated using a 7560 base clone of the single-stranded M13MP18 bacteriophage viral genome[5] and 160 single-stranded staples that were ordered from a commercial vendor (Eurofins, Huntsville, AL). Five versions of the compliant joint with varying geometry were designed by varying the length of ssDNA springs (Supporting Information, Figures S7−S11). These versions had 0, 11, 32, 53, and 74 ssDNA bases in the springs, which was achieved by changing only the staples positioned between the ssDNA springs and the loops (∼15% of total staples). For self-assembly, scaffold was mixed at 20 nM with staples at 10-fold excess (each staple at 200 nM) in a folding reaction containing 5 mM Tris, 5 mM NaCl, 1 mM EDTA, and 14−20 mM $MgCl_2$ ($MgCl_2$ concentrations in this range produced similar folding results). The folding reactions were subjected to a thermal annealing ramp where the temperature was quickly increased to 65 °C and then slowly cooled to 4 °C over a time scale of 2.5 days.

Structure Purification and Imaging. DNA origami structures were purified by agarose gel electrophoresis (sample gel image in Supporting Information, Figure S5). Gels were mixed with 2% agarose in 0.5× TBE buffer (44.5 mM Tris-borate, 1 mM EDTA) with 11 mM $MgCl_2$ and 1 μM ethidium bromide. Folded structures were mixed with 6× loading dye (New England Biolabs, Ipswich, MA) and run for approximately 4 h at 70 V. Structure bands were excised and removed from agarose using freeze and squeeze extraction DNA gel extraction spin columns (Biorad, Hercules, CA). To verify proper folding, purified structures were prepared for transmission electron microscopy (TEM) imaging for structural feedback as described in Castro *et al.*[7] Briefly, 4 μL of purified structure solution was deposited on a plasma-treated Formvar-coated TEM grid stabilized with evaporated carbon film (Electron Microscopy Sciences, Hatfield, PA) and incubated for 4 min. The structure solution was wicked away, and structures were negatively stained by applying a 20 μL drop of 2% uranyl formate (SPI, West Chester, PA), incubating for 40 s, and then wicking off the stain solution. Sample grids were allowed to dry for at least 30 min prior to imaging. Images were taken on a FEI Tecnai G2 Spirit TEM at an acceleration voltage of 80 kV.

Conflict of Interest: The authors declare no competing financial interest.

Acknowledgment. This material is based upon work supported by the National Science Foundation under Grant No. CMMI-1235060. Any opinions, findings, and conclusions or recommendations expressed in this material are those of the author(s) and do not necessarily reflect the views of the funding

agency. We also thank the Campus Microscopy and Imaging Facility (CMIF) of Ohio State University.

Supporting Information Available: Detailed derivation of beam model and WLC model equations for our design, detailed production of scaffold, additional TEM images for each version, DNA origami layouts, and staple sequences. This material is available free of charge *via* the Internet at http://pubs.acs.org.

REFERENCES AND NOTES

1. Seeman, N. C. Nanomaterials Based on DNA. *Annu. Rev. Biochem.* **2010**, *79*, 65–87.
2. Seeman, N. C. DNA in a Material World. *Nature* **2003**, *421*, 427–431.
3. Rothemund, P. W. K. Folding DNA To Create Nanoscale Shapes and Patterns. *Nature* **2006**, *440*, 297–302.
4. Dietz, H.; Douglas, S. M.; Shih, W. M. Folding DNA into Twisted and Curved Nanoscale Shapes. *Science* **2009**, *325*, 725–730.
5. Douglas, S. M.; Dietz, H.; Liedl, T.; Högberg, B.; Graf, F.; Shih, W. M. Self-Assembly of DNA into Nanoscale Three-Dimensional Shapes. *Nature* **2009**, *459*, 414–418.
6. Han, D.; Pal, S.; Nangreave, J.; Deng, Z.; Liu, Y.; Yan, H. DNA Origami with Complex Curvatures in Three-Dimensional Space. *Science* **2011**, *332*, 342–346.
7. Castro, C. E.; Kilchherr, F.; Kim, D.-N.; Shiao, E. L.; Wauer, T.; Wortmann, P.; Bathe, M.; Dietz, H. A Primer to Scaffolded DNA Origami. *Nat. Methods* **2011**, *8*, 221–229.
8. Linko, V.; Dietz, H. The Enabled State of DNA Nanotechnology. *Curr. Opin. Biotechnol.* **2013**, *24*, 555–561.
9. Langecker, M.; Arnaut, V.; Martin, T. G.; List, J.; Renner, S.; Mayer, M.; Dietz, H.; Simmel, F. C. Synthetic Lipid Membrane Channels Formed by Designed DNA Nanostructures. *Science* **2012**, *338*, 932–936.
10. Douglas, S. M.; Bachelet, I.; Church, G. M. A Logic-Gated Nanorobot for Targeted Transport of Molecular Payloads. *Science* **2012**, *335*, 831–834.
11. Zadegan, R. M.; Jepsen, M. D. E.; Thomsen, K. E.; Okholm, A. H.; Schaffert, D. H.; Andersen, E. S.; Birkedal, V.; Kjems, J. Construction of a 4 Zeptoliters Switchable 3D DNA Box Origami. *ACS Nano* **2012**, *6*, 10050–10053.
12. Douglas, S. M.; Chou, J. J.; Shih, W. M. DNA-Nanotube-Induced Alignment of Membrane Proteins for NMR Structure Determination. *Proc. Natl. Acad. Sci. U.S.A.* **2007**, *104*, 6644–6648.
13. Schreiber, R.; Kempter, S.; Holler, S.; Schüller, V.; Schiffels, D.; Simmel, S. S.; Nickels, P. C.; Liedl, T. DNA Origami-Templated Growth of Arbitrarily Shaped Metal Nanoparticles. *Small* **2011**, *7*, 1795–1799.
14. Ding, B.; Deng, Z.; Yan, H.; Cabrini, S.; Zuckermann, R. N.; Bokor, J. Gold Nanoparticle Self-Similar Chain Structure Organized by DNA Origami. *J. Am. Chem. Soc.* **2010**, *132*, 3248–3249.
15. Maune, H. T.; Han, S.; Barish, R. D.; Bockrath, M.; Iii, W. A. G.; Rothemund, P. W. K.; Winfree, E. Self-Assembly of Carbon Nanotubes into Two-Dimensional Geometries Using DNA Origami Templates. *Nat. Nanotechnol.* **2010**, *5*, 61–66.
16. Derr, N. D.; Goodman, B. S.; Jungmann, R.; Leschziner, A. E.; Shih, W. M.; Reck-Peterson, S. L. Tug-of-War in Motor Protein Ensembles Revealed with a Programmable DNA Origami Scaffold. *Science* **2012**, *338*, 662–665.
17. Douglas, S. M.; Marblestone, A. H.; Teerapittayanon, S.; Vazquez, A.; Church, G. M.; Shih, W. M. Rapid Prototyping of 3D DNA-Origami Shapes with caDNAno. *Nucleic Acids Res.* **2009**, *37*, 5001–5006.
18. Kim, D.-N.; Kilchherr, F.; Dietz, H.; Bathe, M. Quantitative Prediction of 3D Solution Shape and Flexibility of Nucleic Acid Nanostructures. *Nucleic Acids Res.* **2012**, *40*, 2862–2868.
19. Wolfe, K. C.; Hastings, W. A.; Dutta, S.; Long, A.; Shapiro, B. A.; Woolf, T. B.; Guthold, M.; Chirikjian, G. S. Multiscale Modeling of Double-Helical DNA and RNA: A Unification through Lie Groups. *J. Phys. Chem. B* **2012**, *116*, 8556–8572.
20. Yamakawa, H. *Helical Wormlike Chains in Polymer Solutions*; Springer: Berlin, 1997.
21. Odijk, T. Stiff Chains and Filaments under Tension. *Macromolecules* **1995**, *28*, 7016–7018.
22. Marko, J. F.; Siggia, E. D. Stretching DNA. *Macromolecules* **1995**, *28*, 8759–8770.
23. Fu, J.; Yan, H. Controlled Drug Release by a Nanorobot. *Nat. Biotechnol.* **2012**, *30*, 407–408.
24. Elbaz, J.; Willner, I. DNA Origami: Nanorobots Grab Cellular Control. *Nat. Mater.* **2012**, *11*, 276–277.
25. Bath, J.; Turberfield, A. J. DNA Nanomachines. *Nat. Nanotechnol.* **2007**, *2*, 275–284.
26. Su, H.-J.; Castro, C. E.; Marras, A. E.; Hudoba, M. Design and Fabrication of DNA Origami Mechanisms and Machines. In *Advances in Reconfigurable Mechanisms and Robots I*; Springer: London, 2012; pp 487−500.
27. Tinland, B.; Pluen, A.; Sturm, J.; Weill, G. Persistence Length of Single-Stranded DNA. *Macromolecules* **1997**, *30*, 5763–5765.
28. Kauert, D. J.; Kurth, T.; Liedl, T.; Seidel, R. Direct Mechanical Measurements Reveal the Material Properties of Three-Dimensional DNA Origami. *Nano Lett.* **2011**, *11*, 5558–5563.
29. Cohen, A. E.; Moerner, W. E. Principal-Components Analysis of Shape Fluctuations of Single DNA Molecules. *Proc. Natl. Acad. Sci. U.S.A.* **2007**, *104*, 12622–12627.
30. Culpepper, M. L.; DiBiasio, C. M.; Panas, R. M.; Magleby, S.; Howell, L. L. Simulation of a Carbon Nanotube-Based Compliant Parallel-Guiding Mechanism: A Nanomechanical Building Block. *Appl. Phys. Lett.* **2006**, *89*, 203111/1–203111/3.
31. Magleby, S. P.; Culpepper, M. L.; Howell, L. L.; Panas, R.; DiBiasio, C. M. Comparison of Molecular Simulation and Pseudo-Rigid-Body Model Predictions for a Carbon Nanotube-Based Compliant Parallel-Guiding Mechanism. *J. Mech. Des.* **2008**, *130*, 042308/1–042308/7.
32. Howell, L. L; Midha, A. A Method for the Design of Compliant Mechanisms with Small-Length Flexural Pivots. *J. Mech. Des.* **1994**, *116*, 280–290.
33. Howell, L. L. *Compliant Mechanisms*; Wiley-Interscience: New York, 2001; pp 10−18.
34. Reckmann, B.; Grosse, F.; Urbanke, C.; Frank, R.; Blöcker, H.; Krauss, G. Analysis of Secondary Structures in M13mp8(+) Single-Stranded DNA by the Pausing of DNA Polymerase α. *Eur. J. Biochem.* **1985**, *152*, 633–643.
35. Dong, F.; Allawi, H. T.; Anderson, T.; Neri, B. P.; Lyamichev, V. I. Secondary Structure Prediction and Structure-Specific Sequence Analysis of Single-Stranded DNA. *Nucleic Acids Res.* **2001**, *29*, 3248–3257.
36. Protozanova, E.; Yakovchuk, P.; Frank-Kamenetskii, M. D. Stacked−Unstacked Equilibrium at the Nick Site of DNA. *J. Mol. Biol.* **2004**, *342*, 775–785.
37. Zhou, Y.; Chirikjian, G. S. Conformational Statistics of Semi-flexible Macromolecular Chains with Internal Joints. *Macromolecules* **2006**, *39*, 1950–1960.
38. Zhou, Y.; Chirikjian, G. S. Conformational Statistics of Bent Semiflexible Polymers. *J. Chem. Phys.* **2003**, *119*, 4962–4970.
39. Kratky, O.; Porod, G. X-ray Investigation of Dissolved Chain Molecules. *Recl. Trav. Chim. Pays-Bas* **1949**, *68*, 1106–1122.
40. Baumann, C. G.; Smith, S. B.; Bloomfield, V. A.; Bustamante, C. Ionic Effects on the Elasticity of Single DNA Molecules. *Proc. Natl. Acad. Sci. U.S.A.* **1997**, *94*, 6185–6190.
41. Bustamante, C.; Smith, S. B.; Liphardt, J.; Smith, D. Single-Molecule Studies of DNA Mechanics. *Curr. Opin. Struct. Biol.* **2000**, *10*, 279–285.
42. Manning, G. S. The Persistence Length of DNA Is Reached from the Persistence Length of Its Null Isomer through an Internal Electrostatic Stretching Force. *Biophys. J.* **2006**, *91*, 3607–3616.
43. Beer, F. P.; Johnston, E. R.; DeWolf, J. T. *Mechanics of Materials*, 3rd ed.; McGraw-Hill Science/Engineering/Math: New York, 2001; pp 670−733.
44. Blanchoin, L.; Amann, K. J.; Higgs, H. N.; Marchand, J.-B.; Kaiser, D. A.; Pollard, T. D. Direct Observation of Dendritic Actin Filament Networks Nucleated by Arp2/3 Complex and WASP/Scar Proteins. *Nature* **2000**, *404*, 1007–1011.

45. Hartemink, C. A. The Cross-Linking Mechanism of Filamin A in the Actin Cytoskeleton. Ph.D. Thesis, Massachusetts Institute of Technology, June 2005.
46. Endo, M.; Yang, Y.; Sugiyama, H. DNA Origami Technology for Biomaterials Applications. *Biomater. Sci.* **2013**, *1*, 347–360.
47. Liu, W.; Zhong, H.; Wang, R.; Seeman, N. C. Crystalline Two-Dimensional DNA-Origami Arrays. *Angew. Chem., Int. Ed.* **2011**, *50*, 264–267.
48. Lieleg, O.; Claessens, M. M.; Bausch, A. R. Structure and Dynamics of Cross-Linked Actin Networks. *Soft Matter* **2010**, *6*, 218–225.
49. Smith, S. B.; Cui, Y.; Bustamante, C. Overstretching B-DNA: The Elastic Response of Individual Double-Stranded and Single-Stranded DNA Molecules. *Science* **1996**, *271*, 795–799.
50. Crozier, P. S.; Stevens, M. J. Simulations of Single Grafted Polyelectrolyte Chains: ssDNA and dsDNA. *J. Chem. Phys.* **2003**, *118*, 3855–3860.
51. Chi, Q.; Wang, G.; Jiang, J. The Persistence Length and Length per Base of Single-Stranded DNA Obtained from Fluorescence Correlation Spectroscopy Measurements Using Mean Field Theory. *Phys. A (Amsterdam, Neth.)* **2013**, *392*, 1072–1079.
52. Murphy, M. C.; Rasnik, I.; Cheng, W.; Lohman, T. M.; Ha, T. Probing Single-Stranded DNA Conformational Flexibility Using Fluorescence Spectroscopy. *Biophys. J.* **2004**, *86*, 2530–2537.
53. Watson, J. D.; Crick, F. H. Molecular Structure of Nucleic Acids. *Nature* **1953**, *171*, 737–738.
54. Mandelkern, M.; Elias, J. G.; Eden, D.; Crothers, D. M. The Dimensions of DNA in Solution. *J. Mol. Biol.* **1981**, *152*, 153–161.